



1 **Improving hydrological projection performance under contrasting**  
2 **climatic conditions using spatial coherence through a hierarchical**  
3 **Bayesian regression framework**

4 **Zhengke Pan<sup>a,b</sup>, Pan Liu<sup>a,b,\*</sup>, Shida Gao<sup>a,b</sup>, Jun Xia<sup>a,b,c</sup>, Jie Chen<sup>a,b</sup>, Lei Cheng<sup>a,b</sup>**

5

6 <sup>a</sup>State Key Laboratory of Water Resources and Hydropower Engineering Science, Wuhan University,

7 Wuhan 430072, China

8

9 <sup>b</sup>Hubei Provincial Collaborative Innovation Center for Water Resources Security, Wuhan 430072,

10 China

11 <sup>c</sup>Chinese Academy of Sciences, Beijing 100864, China

12

13 <sup>\*</sup>Corresponding author. Email: [liupan@whu.edu.cn](mailto:liupan@whu.edu.cn); Tel: +86-27-68775788; Fax: +86-27-68773568

14

15

16

17

18

19

20

21

22



23 **ABSTRACT**

24 Understanding the projection performance of hydrological models under contrasting  
25 climatic conditions supports robust decision making, which highlights the need to adopt  
26 time-varying parameters in hydrological modeling to reduce the performance  
27 degradation. Many existing literatures model the time-varying parameters as functions  
28 of physically-based covariates; however, a major challenge remains finding effective  
29 information to control the large uncertainties that are linked to the additional parameters  
30 within the functions. This paper formulated the time-varying parameters for a lumped  
31 hydrological model as explicit functions of temporal covariates and used a hierarchical  
32 Bayesian (HB) framework to incorporate the spatial coherence of adjacent catchments  
33 to improve the robustness of the projection performance. Four modeling scenarios with  
34 different spatial coherence schemes, and one scenario with a stationary scheme for  
35 model parameters, were used to explore the transferability of hydrological models  
36 under contrasting climatic conditions. Three spatially adjacent catchments in southeast  
37 Australia were selected as case studies to examine validity of the proposed method.  
38 Results showed that (1) the time-varying function improved the model performance but  
39 also amplified the projection uncertainty compared with stationary setting of model  
40 parameters; (2) the proposed HB method successfully reduced the projection  
41 uncertainty and improved the robustness of model performance; and (3) model  
42 parameters calibrated over dry periods were not suitable for predicting runoff over wet  
43 periods because of a large degradation in projection performance. This study improves  
44 our understanding of the spatial coherence of time-varying parameters, which will help  
45 improve the projection performance under differing climatic conditions.

46 **Keywords:** Climate change; Hierarchical Bayesian; Hydrological model parameters;  
47 Spatial coherence; Streamflow projection; Contrasting climatic conditions

48  
49



## 50 1. INTRODUCTION

51 Long-term streamflow projection is an important part of effective water resources  
52 planning because it can predict future scarcity in water supply and help prevent floods.  
53 Streamflow projections typically involve the following: (i) calibrating hydrological  
54 model parameters with partial historical observations (e.g., precipitation, evaporation  
55 and streamflow); (ii) projecting streamflow under periods that are outside of those for  
56 model calibration; and (iii) evaluating the model projection performance with certain  
57 criteria. One of the most basic assumptions of this process—that the calibrated model  
58 parameters are stationary and can be applied to predict catchment behaviors in the near  
59 future, has been widely questioned (Brigode et al., 2013; Broderick et al., 2016; Chiew  
60 et al., 2014; Chiew et al., 2009; Ciais et al., 2005; Clarke, 2007; Cook et al., 2004; Coron  
61 et al., 2012; Deng et al., 2016; Merz et al., 2011; Moore and Wondzell, 2005; Moradkhani  
62 et al., 2012; Moradkhani et al., 2005; Pathiraja et al., 2016; Pathiraja et al., 2018; Patil and  
63 Stieglitz, 2015; Westra et al., 2014; Xiong et al., 2019; Zhang et al., 2018).

64 Many previous studies have explored the transferability of stationary parameters  
65 to periods with different climatic conditions. They have concluded that hydrological  
66 model parameters are sensitive to the climatic conditions of the calibration period  
67 (Chiew et al., 2014; Chiew et al., 2009; Coron et al., 2012; Merz et al., 2011; Renard et  
68 al., 2011; Seiller et al., 2012; Vaze et al., 2010). For instance, Merz et al. (2011)  
69 calibrated model parameters using six consecutive 5-year periods between 1976 and  
70 2006 for 273 catchments in Austria and found that the calibrated parameters  
71 representing snow and soil moisture processes showed significant trend in the study



72 area. Other studies have found that degradation in model performance was directly  
73 related to the difference in precipitation between calibration and verification periods  
74 (Coron et al., 2012; Vaze et al., 2010). One proposal for managing this problem is to  
75 calibrate model parameters in periods with similar climatic conditions to the near future,  
76 but future streamflow observations are unavailable. Thus, it is still necessary to reduce  
77 the magnitude of performance loss and improve the robustness of the projection  
78 performance using calibrated parameters based on the historical records, even though  
79 the climatic conditions in the future may be dissimilar to those used for model  
80 calibration.

81 Several recent studies have found that hydrological models with time-varying  
82 parameters exhibited a significant improvement in its projection performance compared  
83 with the stationary parameters (Deng et al., 2016; Deng et al., 2018; Westra et al., 2014).  
84 The functional method is one of the most promising ways to model time-varying  
85 parameters and shows its excellence in improving the model projection performance  
86 (Guo et al., 2017; Westra et al., 2014; Wright et al., 2015). This method models the time-  
87 varying parameter(s) as function(s) of physically-based covariates (e.g., temporal  
88 covariate and Normalized Difference Vegetation Index). Generally, the hydrological  
89 model is run with various assumed functions, the best functional forms of time-varying  
90 parameters can be obtained by comparing the evaluation criteria. However, a major  
91 challenge for the application of the functional method remains finding effective  
92 information to control the large uncertainties that are linked to the additional parameters  
93 describing these regression functions.



94 Similarity of adjacent catchments, has been verified its validity in controlling the  
95 estimation uncertainty of model parameters (Bracken et al., 2018;Cha et al.,  
96 2016;Cooley et al., 2007;Lima and Lall, 2009;Najafi and Moradkhani, 2014;Sun and  
97 Lall, 2015;Sun et al., 2015;Yan and Moradkhani, 2015). The level of similarity of  
98 different catchments is known as spatial coherence. For instance, Sun and Lall (2015)  
99 used the spatial coherence of trends in annual maximum precipitation in the United  
100 States, and successfully reduced the parameter estimation uncertainty in their at-site  
101 frequency analysis. In general, there are three methods to consider the spatial coherence  
102 between different catchments in parameter estimation, i.e., no pooling, complete  
103 pooling and hierarchical Bayesian (HB) framework (also known as partial pooling). In  
104 these three approaches, the HB framework has been proved as the most efficient method  
105 to incorporate the spatial coherence to reduce the estimation uncertainty because it has  
106 the advantage of shrinking the local parameter toward the common regional mean and  
107 including an estimation of its variance or covariance across the catchments (Bracken et  
108 al., 2018;Sun and Lall, 2015;Sun et al., 2015). In the field of hydrological modeling,  
109 most proceeding literatures were focused on no pooling models that neglect the spatial  
110 coherence between catchments (Heuvelmans et al., 2006;Lebecherel et al., 2016;Merz  
111 and Blöschl, 2004;Oudin et al., 2008;Singh et al., 2012;Tegegne and Kim, 2018;Xu et  
112 al., 2018); little attention has been paid to the HB framework. Thus, we want to fill this  
113 gap and explore the applicability of the spatial coherence through the HB framework in  
114 hydrological modeling with the time-varying parameters.

115 The objectives of this paper were to: (1) verify the effect of the time-varying model



116 parameter scheme on model projection performance and uncertainty analysis compared  
117 with stationary model parameters; (2) verify the projection performance of considering  
118 spatial coherence of adjacent catchments through the HB framework compared with  
119 spatial incoherence; and (3) compare the model projection performance for different  
120 climatic transfer schemes.

121 This paper is organized as follows. Section 2 introduces the differential split  
122 sample test (DSST) for segmenting the historical series, the hydrological model, and  
123 the two-level HB framework for incorporating spatial coherence from adjacent  
124 catchments. Section 3 provides a case study of the proposed methodology for improving  
125 hydrological projection performance under contrasting climatic conditions. Section 4  
126 summarizes the main conclusions of the study.

## 127 2. METHODOLOGY

128 The methodology is outlined by a flowchart in Figure 1, and is summarized as  
129 follows:

130 (1) A temporal parameter transfer scheme is implemented (described in section 2.1)  
131 using a classic DSST procedure in which the available data are divided into non-dry  
132 and dry periods;

133 (2) A daily conceptual rainfall-runoff model is used (outlined in section 2.2);

134 (3) A two-level HB framework is used to incorporate spatial coherence in  
135 hydrological modeling (described in section 2.3). The data level (first level) of the  
136 framework models the temporal variation in the model parameters using a time-varying  
137 function, while the process level (second level) models the spatial coherence of the



138 regression parameters in the time-varying function. Four modeling scenarios with  
139 different spatial coherence schemes, and one scenario with a stationary scheme for the  
140 model parameter, are used to evaluate the transferability of hydrological models under  
141 contrasting climatic conditions;

142 (4) Likelihood function and parameter estimation methods are applied (outlined in  
143 section 2.4); and

144 (5) The criteria are used to evaluate the model performance for various model  
145 scenarios (described in section 2.5).

## 146 **2.1 Differential split sampling test**

147 To verify the projection performance of the rainfall-runoff model under contrasting  
148 climatic conditions (non-dry and dry periods), a classic DSST using annual rainfall  
149 records was adopted.

### 150 **2.1.1 Dry period identification**

151 Two separate tasks were needed to develop the DSST method into a working  
152 system. The first step was to define the “dry period”. The method to define the dry  
153 period is adopted from Saft et al. (2015), and is a rigorous identification method that  
154 treats autocorrelation in the regression residuals, undertakes global significance testing,  
155 and defines the start and end of the droughts individually for each catchment. In the  
156 second step, the non-dry period was defined as the complement of the dry period in the  
157 historical records. A similar approach to define the dry and non-dry periods was used  
158 by Fowler et al. (2016).



159 2.1.2 Verification method

160 In the DSST method, the model parameters calibrated in the non-dry period were  
161 evaluated in the dry period, and vice versa. The projection performance of the calibrated  
162 parameters for different transfer schemes was evaluated using the criteria illustrated in  
163 section 2.5.

164 **2.2 The rainfall-runoff model**

165 The hydrological model used in this study is the GR4J (modèle du Génie Rural à  
166 4 paramètres Journalier), which is a lumped conceptual rainfall-runoff model (Perrin et  
167 al., 2003). The original version of the GR4J model (Figure 2) comprised four  
168 parameters (Perrin et al., 2003): production store capacity ( $\theta_1$  mm), groundwater  
169 exchange coefficient ( $\theta_2$  mm), 1-day-ahead maximum capacity of the routing store ( $\theta_3$   
170 mm), and the time base of the unit hydrograph ( $\theta_4$  days). More details on the GR4J  
171 model can be found in Perrin et al. (2003).

172 The GR4J model is a parsimonious, but efficient model. The model has been used  
173 successfully across a wide range of hydro-climatic conditions across the world,  
174 including the crash testing of model performance under contrasting climatic conditions  
175 (Coron et al., 2012), and the simulation of runoff for revisiting the deficiency in  
176 insufficient model calibration (Fowler et al., 2016). In addition, Fowler et al. (2016)  
177 verified that conceptual rainfall-runoff models were more capable under changing  
178 climatic conditions than previously thought. These characteristics make the GR4J  
179 particularly suitable as a starting point for implementing modifications and/or  
180 improving predictive ability under changing climatic conditions.





## 181 **2.3 The HB framework for the time-varying model parameter**

182 In this study, various versions were constructed for evaluating the projection  
183 capabilities of models for contrasting climatic conditions (non-dry and dry periods),  
184 and for considering the temporal variation and spatial coherence of parameter  $\theta_1$ .

### 185 2.3.1 Data level: temporal variation of the model parameter

186 As described in the literature (Perrin et al., 2003;Renard et al., 2011;Westra et  
187 al., 2014), the parameter  $\theta_1$ , which represents the primary storage of water in the  
188 catchment, is the most sensitive parameter in the GR4J model structure, and  
189 stochastic variations of this parameter have the largest impact on model projection  
190 performance (Renard et al., 2011;Westra et al., 2014). In addition, the temporal  
191 variation in the catchment storage capacity was physically interpretable. Periodic  
192 variations in the production store capacity  $\theta_1$  can be induced by the periodicity in  
193 precipitation and in seasonal vegetation growth and senescence. In the present study,  
194  $\theta_1$  was constructed to account for the periodical variation that had a significant impact  
195 on the extensionality of the model. The periodical variation in catchment storage  
196 capacity  $\theta_1$  is described by a sine function, using amplitude and phase.

197 Thus, for any catchment  $c$ , the full temporal regression function for  $\theta_1$  at the data  
198 level is:

$$199 \quad \text{Data level:} \quad \theta_1(c) = \alpha(c) + \beta(c) \sin[\omega(c)t] \quad (1)$$

200 where  $\alpha$ ,  $\beta$ ,  $\omega$  are regression parameters for the specific DSST method, and  $\alpha$   
201 signifies the intercept, and  $\{\beta, \omega\}$  represents the amplitude and phase of the sine  
202 function, respectively. If model parameter  $\theta_1$  is constant then  $\alpha=\beta=\omega=0$  suffices



203 in Eq.1 and the resulting model simplifies to a stationary hydrological model.

204

### 205 2.3.2 Process level: spatial coherence of regression parameters

206 For a heterogeneous region that is distinctly non-uniform in climatic and geologic  
207 conditions, different catchments within the region typically have different catchment  
208 storage capacities and different values of production store capacity  $\theta_1$ . For a  
209 homogeneous region prescribed by similar climatic and geologic conditions in each  
210 part, the production store capacity (in Eq. 2) is expected to be the same among different  
211 catchments of the region. The model could be improved by considering spatial input,  
212 i.e., the spatial coherence of parameters across adjacent catchments (Chen et al.,  
213 2014; Lima et al., 2016; Merz and Blöschl, 2004; Oudin et al., 2008; Patil and Stieglitz,  
214 2015; Renard et al., 2011; Sun et al., 2014).

215 At the process level, independent Gaussian prior distributions were used for the  
216 regression parameters  $\{\beta, \omega\}$  as follows:

217 Process level:

$$\begin{aligned} \beta(c) &= N(\mu_2, \sigma_2^2) \\ \omega(c) &= N(\mu_3, \sigma_3^2) \end{aligned} \quad (2)$$

218 where  $\mu_2, \mu_3, \sigma_2$  and  $\sigma_3$  are hyper-parameters, and  $N(\cdot)$  represents the  
219 hyper-distribution, i.e., a Gaussian distribution. Independent Gaussian distributions  
220 were assumed for the regression parameters  $\{\beta, \omega\}$  that were used to model spatial  
221 coherence based on practical considerations. The process level of the HB framework  
222 aims to describe the variation of  $\{\beta, \omega\}$  in space by means of a Gaussian spatial  
223 process in which the mean value depends on covariates describing regional



224 characteristics. Regression parameters  $\beta$  and  $\omega$  are the most important parameters  
225 in the regression function and can reflect the spatial connection of variation and  
226 cyclicity of catchment production storage capacity among catchments. A similar setting  
227 was made in Sun and Lall (2015) and Sun et al. (2015).

### 228 2.3.3 Modeling scenarios

229 Five modeling scenarios (Table 1) were carried out to assess the effect of spatial  
230 coherence on the time-varying function. Different levels of spatial coherence of  
231  $\{\beta, \omega\}$  were assumed in scenarios 1 to 4, while in scenario 5 parameter  $\theta_1$  was set  
232 to be constant to provide a comparison.

## 233 2.4 Estimation and projection

234 The objective function and parameter inference methods were used to derive the  
235 posterior distribution of all unknown quantities, as illustrated below.

### 236 2.4.1 Likelihood function

237 For a specific catchment, the model parameters were calibrated to minimize the  
238 following objective function, which was adopted from Coron et al. (2012).

$$239 \quad \varepsilon_c = -RMSE[\sqrt{Q}](1 + |BIAS|) \quad (3)$$

240 where

$$241 \quad RMSE[\sqrt{Q}] = \sqrt{\frac{1}{T} \sum_{t=1}^T [Q_{sim}(t) - Q_{obs}(t)]^2} \quad (4)$$

242 and  $RMSE[\sqrt{Q}]$  refers to the root-mean-square error.

243 Coron et al. (2012) showed that this objective function performed well. In this  
244 function, the combination of  $RMSE[\sqrt{Q}]$  and  $BIAS$  (Eq.7) gives weight to dynamic  
245 representation as well as the water balance. Using square-root-transformed flows to



246 compute the RMSE reduces the influence of high flows during the calibration period  
247 and provides a good compromise between alternative criteria.

248 In the case of multiple catchments, the objective function of the HB framework  
249 was written as follows:

$$250 \quad \Lambda = \prod_{c=1}^C \varepsilon_c \cdot \prod_{n=1}^2 f_N(\beta, \omega | \mu_2, \sigma_2, \mu_3, \sigma_3) \quad (5)$$

251 where the number of catchments in the region is represented by  $C$ , and the Gaussian  
252 spatial function between regression parameters  $\beta, \omega$  and hyper-parameters  $\mu_2, \mu_3,$   
253  $\sigma_2$  and  $\sigma_3$  are denoted by  $f_N()$ .

#### 254 2.4.2 Inference

255 The likelihood functions defined in Eqs. 3 and 5 pose a computational challenge  
256 because their dimensionality grows (primarily related to the number of catchment-  
257 specific parameters) with the number of catchments considered. The unknown  
258 parameters are estimated using the Shuffled Complex Evolution Metropolis (SCEM-  
259 UA) sampling method (Ajami et al., 2007; Vrugt et al., 2003; Vrugt et al., 2009), which  
260 is a widely used Markov Chain Monte Carlo algorithm for simulating the posterior  
261 probability distribution of parameters that are conditional on the current choice of  
262 parameters and data. When compared with traditional Metropolis-Hasting samplers, the  
263 SCEM-UA algorithm more efficiently reduces the number of model simulations needed  
264 to infer the posterior distribution of parameters, (Ajami et al., 2007; Duan et al.,  
265 2007; Liu et al., 2014; Liu and Gupta, 2007; Vrugt et al., 2003). Convergence is assessed  
266 by evolving three parallel chains, while verifying that the posterior distribution of  
267 parameters results in a value smaller than a Gelman-Rubin convergence value of 1.2



268 (Gelman et al., 2013).

## 269 **2.5 Model performance criteria**

270 Three criteria were used to assess the projection performance for the verification  
271 periods.

272 (1) The first criterion was  $NSE_{sqr}$ , known as the arithmetic square root of Nash-  
273 Sutcliffe Efficiency (Coron et al., 2012; Moriasi et al., 2007; Nash and Sutcliffe, 1970).

274 When compared with the classic NSE,  $NSE_{sqr}$  gives an intermediate, more balanced  
275 picture of the overall hydrograph fit because it can reduce the influence of high flow. It  
276 is expressed as:

$$277 \quad NSE_{sqr} = 1 - \frac{\sum_{t=1}^T [\sqrt{Q_{obs}(t)} - \sqrt{Q_{sim}(t)}]^2}{\sum_{t=1}^T [\sqrt{Q_{obs}(t)} - \sqrt{\bar{Q}_{obs}}]^2} \quad (6)$$

278 where  $Q_{sim}(t)$  and  $Q_{obs}(t)$  represent the simulated and observed daily streamflow  
279 values for the  $t^{\text{th}}$  day, respectively;  $\bar{Q}_{obs}$  is the mean of the observed daily streamflow  
280 for the calculation interval; and  $T$  refers to the length of the calculation period.

281 (2) The second criterion is the BIAS, which is a part of the objective function.

$$282 \quad BIAS = \frac{\sum_{t=1}^T [Q_{sim}(t) - Q_{obs}(t)]}{\sum_{t=1}^T [Q_{obs}(t)]} \quad (7)$$

283 (3) The third criterion is the Deviance information criterion (DIC), which was  
284 defined by Spiegelhalter et al. (2002). It is a widely used and popular measure designed  
285 for Bayesian model comparison and is a Bayesian alternative to the standard Akaike  
286 Information Criterion. The DIC value for a Bayesian scenario is obtained as:



287 
$$DIC = -2 \log \left( p \left( q | \theta_{Bayes}, \xi \right) \right) + 2 p_{DIC} \quad (8)$$

288 where  $p_{DIC}$  is the effective number of parameters, defined as

289 
$$p_{DIC} = 2 \left( \log \left( p \left( q | \theta_{Bayes}, \xi \right) \right) - \frac{1}{S} \sum_{s=1}^S \log \left( p \left( q | \theta^s, \xi \right) \right) \right) \quad (9)$$

290 where posterior mean  $\theta_{Bayes} = \text{Expect}(\theta | q, \xi)$  and  $s=1, \dots, S$ , means the sequence  
291 number of the simulated parameter set  $\theta^s$  by the adopted SCEM-UA algorithm.  
292 According to Spiegelhalter et al. (2002), scenarios with smaller DIC would be preferred  
293 to scenarios with larger DIC.

### 294 3. CASE STUDY

#### 295 3.1 Study area and data

296 To evaluate the model performance, we used daily precipitation (mm/day),  
297 evapotranspiration (mm/day), and streamflow (mm/day) time series records for three  
298 unregulated and unimpaired catchments in south-eastern Australia, taken from the  
299 national dataset of Australia (Zhang et al., 2013), covering 1976–2011. The streams  
300 were unregulated: they were not subject to dam or reservoir regulations, which can  
301 reduce the impact of human activity. The observed streamflow record contained at least  
302 11835 daily observations (equivalent to a record integrity of greater than 90%) for  
303 1976–2011, with acceptable data quality. The first complete year of data was used for  
304 model warm-up to reduce the impact of the initial soil moisture conditions during the  
305 calibration period.

306 The attributes of the south-eastern Australian catchments are shown in Table 2 and  
307 Figure 3. The IDs of these catchments are 225219 (Glencairn station on the Macalister



308 River: mean annual rainfall, potential evapotranspiration, and runoff are 1064 mm,  
309 1142 mm, and 350 mm, respectively), 405219 (Dohertys station on the Goulburn river:  
310 mean annual rainfall, potential evapotranspiration, and runoff are 1169 mm, 1193 mm,  
311 and 422 mm, respectively), and 405264 (D/S of Frenchman Ck Jun station on the Big  
312 river: mean annual rainfall, potential evapotranspiration, and runoff are 1406 mm, 1157  
313 mm, and 469 mm, respectively). These catchments are adjacent to each other and satisfy  
314 the homogeneity assumption. All catchments experienced a severe multiyear drought  
315 around the end of the millennium. Saft et al. (2015) identified that the rainfall-runoff  
316 relationship in these catchments was altered during the long-term drought.

### 317 **3.2 Results and discussion**

318 Results from the DSST were used to assess the model projection performance for  
319 five scenarios under contrasting climatic conditions. First, a DSST was conducted in  
320 each catchment to divide original records into non-dry and dry periods. Then, the  
321 projection performance for the five scenarios and associated parameter uncertainties  
322 were evaluated using the criteria described above.

#### 323 **3.2.1 Dry period identification**

324 As illustrated in Table 3 and Figure 4, the drought definition method identified that  
325 the three catchments had similar dry period characteristics, with the same drought start  
326 (1997) and end (2009) points. The mean dry period anomaly was less severe in the  
327 Macalister catchment (225219), with a 6.95% reduction in the mean dry period anomaly  
328 while the other two catchments experienced reductions of 9.84% (405219) and 9.62%  
329 (405264).



330 In terms of changes in rainfall, both catchments had a reduction from the non-dry  
331 to the dry periods of 11% on average, which was within the range that Vaze et al. (2010)  
332 recommended for acceptable model simulations. Vaze et al. (2010) tested four  
333 conceptual rainfall-runoff models in 61 catchments in southeast Australia using the  
334 stationary scheme of model parameters, and found that the calibrated parameter sets  
335 generally gave acceptable simulations provided rainfall changes were not too large (no  
336 more than 15% dryer or 20% wetter than rainfall in the calibration period).

### 337 3.2.2 Model performance in five scenarios

338 Generally, the calibrated model parameters provided good simulation performance  
339 over the calibrated periods for all criteria (Broderick et al., 2016; Coron et al.,  
340 2012; Fowler et al., 2016; Thirel et al., 2015; Vaze et al., 2010). For example, the mean  
341  $NSE_{\text{sqr}}t$  score during the calibration period across these catchments remained close to  
342 about 0.7 or slightly higher, regardless of which scenario was chosen. However, when  
343 the same parameter sets were verified by simulating streamflow over drier or wetter  
344 periods, the model performance was degraded, including both the robustness and  
345 accuracy of projection performance. Furthermore, the magnitude of performance loss  
346 increases along with the variation between the calibration and verification periods.

347 Figure 5 shows the  $NSE_{\text{sqr}}t$  performance for calibration in a non-dry period and  
348 verification in a dry period for each scenario in all catchments. All scenarios performed  
349 well in all catchments with the mean  $NSE_{\text{sqr}}t$  reaching 0.81 during the non-dry  
350 calibration period, and then all scenarios experienced a slight decrease in performance  
351 ( $NSE_{\text{sqr}}t = 0.75$ ) during the dry verification period. Scenario 4 (time-varying parameters





352 without spatial inputs) and scenario 5 (temporally stable parameters) generally  
353 performed better during the calibration period than the scenarios that considered  
354 different levels of spatial coherence for the regression parameters. During the  
355 verification period, the  $NSE_{\text{sqr}}t$  rank order changed (Figure 5b). Scenario 4 had a higher  
356 median  $NSE_{\text{sqr}}t$  performance, but a wider variation range, than scenario 5, which  
357 indicates the validity of the time-varying scheme for improving the model performance.  
358 However, the introduction of additional regression parameters ( $\alpha, \beta$  and  $\omega$ ) at the  
359 same time amplified the model projection uncertainty. Fortunately, the appropriate  
360 adoption of spatial coherence alleviates this problem. Scenario 3, which considered  
361 spatial coherence of regression parameters  $\beta$  and  $\omega$  between different catchments,  
362 exhibited the highest median  $NSE_{\text{sqr}}t$  for all catchments with the smallest fluctuation  
363 range. The highest median  $NSE_{\text{sqr}}t$  performance in scenarios 4 and 5 during the  
364 calibration period did not guarantee the same superior performance during the  
365 verification period. This illustrates the deficiency of time-varying and stationary  
366 schemes of model parameters when spatial inputs from adjacent catchments are not  
367 considered.

368 Similarly, Figure 6 illustrates the  $NSE_{\text{sqr}}t$  performance for each scenario in all  
369 catchments for calibration in the dry period and verification in the non-dry period. All  
370 scenarios performed well for all catchments with the mean  $NSE_{\text{sqr}}t$  reaching 0.75 in the  
371 dry calibration period and 0.79 in the non-dry verification period. As shown in Figure  
372 5, models experienced a slight improvement in  $NSE_{\text{sqr}}t$  performance when transferred  
373 from the dry period to the non-dry period. However, the projection performance



374 calibrated using a contrasting climatic condition was inferior to the simulation  
375 performance that was directly calibrated from the climatic condition. By comparing  
376 scenarios in the calibration period, it was found that scenarios 4 and 5 exhibited the  
377 highest performance, followed successively by scenario 3, scenario 2, and scenario 1.  
378 During the verification period, however, scenario 4 had a higher median  $NSE_{\text{sqrt}}$   
379 performance but a wider variation range than scenario 5, while scenario 3 possessed the  
380 highest median  $NSE_{\text{sqrt}}$  for all catchments with the smallest fluctuation range.

381 These results demonstrate that the time-varying scheme for model parameters  
382 improved the median  $NSE_{\text{sqrt}}$  performance but also amplified the projection uncertainty  
383 compared with the results from the stationary scheme for model parameters. Compared  
384 with other model scenarios, the incorporation of spatial coherence of both regression  
385 parameters in scenario 3 reduced the projection uncertainty and improved the  
386 robustness of the model performance, with the smallest fluctuation ranges under the  
387 contrasting climatic conditions. It indicates that the spatial setting of model parameters  
388 between different catchments provided a clear input for reducing the uncertainty of the  
389 model projection performance during the verification period. In addition, it also should  
390 be noted that model parameters calibrated over dry periods, contrastively, were not  
391 suitable for predicting runoff over wet periods because of a larger degradation in  
392 projection performance than the scheme with the adverse calibration-verification  
393 direction.

394 Compared the DIC results for both DSST schemes in Table 4 and Table 5, the best  
395 DIC value is achieved by scenario 3, which incorporates the spatial coherence of both



396 regression parameters and is the most complex scenario in the comparison. This finding  
397 is consistent with the results by the  $NSE_{sqr}$  criterion, and showed the validity of the  
398 spatial coherence of both regression parameters in ensuring the robustness of the  
399 hydrological projection performance. In addition, when compared DIC results of  
400 scenarios 4 and 5, the setting of time-varying functions improved the DIC performance  
401 in both DSST schemes. This finding also agreed with the results by the  $NSE_{sqr}$  criterion,  
402 and indicated the positive implications by the time-varying model parameters on the  
403 projection performance.

404 Figure 7 shows the BIAS estimates for the median of the posterior distribution of  
405 model parameters for all modeling scenarios across all catchments when transferability  
406 between the non-dry and dry periods was examined. Although the BIAS was a  
407 component of the objective function (Eq. 3), the 10-year rolling average BIAS still  
408 deviated considerably from a value of 1 for all the scenarios in the two DSST schemes.  
409 The median estimates of the posterior distribution in both scenarios performed well in  
410 the  $NSE_{sqr}$  criterion for both periods. However, the median estimates did not ensure  
411 unbiased simulations over the modeling period; one scenario with a higher  $NSE_{sqr}$   
412 criterion may have an altered BIAS during the modeling period. The BIAS results in  
413 catchments 225219 and 405219 showed some similarity: all scenarios tended to  
414 underestimate streamflow along the time sequence in both DSST schemes. Conversely,  
415 all scenarios tended to overestimate the streamflow in catchment 405264 in both  
416 schemes. By comparing the BIAS performance for the five scenarios, it was observed  
417 that the spatial setting of modeling scenarios generally tended to enlarge the BIAS in



418 all catchments, while the difference between scenarios 4 and 5 was very small.

### 419 3.2.3 Parameter uncertainty analysis

420 The uncertainty of the parameters was characterized by the posterior distribution  
421 of the regression parameters and was derived by the MCMC iteration. As mentioned in  
422 section 2.3.2, regression parameters  $\beta$  and  $\omega$  were assumed to have different  
423 levels of spatial coherence in each modeling scenario (Table 1); these scenarios in each  
424 DSST regime are compared in Figs. 7 and 8. It should be mentioned that there was no  
425 regression parameter in scenario 5. Upper and lower ranges in the boxplot are given by  
426 the 25<sup>th</sup> and 75<sup>th</sup> percentiles of the posterior distribution. The whiskers extend to values  
427 defining 1.5-standard deviations of the sample. Small dots (gray) denote the arithmetic  
428 average of the posterior distribution. Values beyond the whiskers are marked as outliers  
429 and denoted as small squares. In the upper plots in Figures 7 and 8, it can be clearly  
430 seen that the first three scenarios had a much smaller variation interval than scenario 4  
431 in terms of regression parameter  $\beta$ , which denotes the amplitude of the sine function.  
432 The median values in the first three scenarios were close to zero while the median  
433 values in the fourth scenario varied significantly between catchments. With regards to  
434 the regression parameter  $\omega$ , which denotes the phase of the sine function (in the lower  
435 figures of Figures 7 and 8), absolute values in the four scenarios differ notably. Scenario  
436 1, which only considered the spatial coherence of the regression parameter  $\omega$ , has the  
437 lowest median value and the narrowest interval for all catchments, followed  
438 successively by scenario 4 (no parameter was spatially coherent) scenario 2 (only  
439 parameter  $\beta$  was spatially coherent), and scenario 3 (both parameters  $\beta$  and  $\omega$



440 were spatially coherent). By considering the spatial coherence of regression parameter  
441  $\omega$  between different catchments it was possible to narrow the variation interval of  
442 posterior distribution (see scenario 1), while adding the spatial coherence of  $\beta$   
443 increased the variation interval of the posterior distribution of  $\omega$  (see scenario 3).

444 In conclusion, by combining the results of parameter uncertainty estimation and  
445 model projection performance evaluation, the incorporation of spatial coherence  
446 successfully improved the robustness of the projection performance in both DSST  
447 schemes by controlling the estimation uncertainty of regression parameters  $\beta$  and  
448  $\omega$ .

#### 449 4. CONCLUSIONS

450 In this study, a two-level HB framework was used to incorporate the spatial  
451 coherence of adjacent catchments to improve the hydrological projection performance  
452 of sensitive time-varying parameters for a lumped conceptual rainfall-runoff model  
453 (GR4J) under contrasting climatic conditions. Firstly, a temporal parameter transfer  
454 scheme was implemented, using a DSST procedure in which the available data were  
455 divided into non-dry and dry periods. Then, the model was calibrated in the non-dry  
456 periods and evaluated in the dry periods, and vice versa. In the first level of the proposed  
457 HB framework, the most sensitive parameter in the GR4J model, i.e., the production  
458 storage capacity ( $\theta_1$ ), was allowed to vary with time to account for the periodic  
459 variation that had significant impacts on the extensionality of the model. The periodic  
460 variation in catchment storage capacity was represented by a sine function for  $\theta_1$   
461 (parameterized by amplitude and phase). In the second level, four modeling scenarios



462 with different spatial coherence schemes, and one scenario with a stationary scheme of  
463 catchment storage capacity, were used to evaluate the transferability of hydrological  
464 models under contrasting climatic conditions. Finally, the proposed method was applied  
465 to three spatially adjacent, unregulated, and unimpaired catchments in southeast  
466 Australia. Results showed that: (1) the time-varying function improved the model  
467 performance but also amplified the projection uncertainty compared with stationary  
468 setting of model parameters; (2) the proposed HB method successfully reduced the  
469 projection uncertainty and improved the robustness of model performance; and (3)  
470 model parameters calibrated over dry periods were not suitable for predicting runoff  
471 over wet periods because of a large degradation in projection performance. This study  
472 improves our understanding of the spatial coherence of time-varying parameters, which  
473 will help improve the projection performance under differing climatic conditions.  
474 However, there are several unsolved problems that need to be addressed. First, the  
475 spatial setting of regression parameters may expand the BIAS between the simulation  
476 and streamflow observation with a single objective function; the potential physical  
477 mechanism behind this result should be explored further. Secondly, this study was  
478 confined to spatially coherent catchments that are similar in climatic and  
479 hydrogeological conditions; further research is needed to determine which factors have  
480 the most significant impacts on model projection performance when considering  
481 obvious inputs from other catchments.

## 482 **ACKNOWLEDGMENTS**

483 This study was supported by the National Key Research and Development



484 Program (2018YFC0407202), the National Natural Science Foundation of China  
485 (51861125102; 51879193), and the Natural Science Foundation of Hubei Province  
486 (2017CFA015). The numerical calculations were done on the supercomputing system  
487 in the Supercomputing Center of Wuhan University. The authors would like to thank  
488 the editor and anonymous reviewers for their comments, which helped improve the  
489 quality of the paper.

#### 490 **AUTHOR CONTRIBUTIONS**

491 All of the authors helped to conceive and design the analysis. Zhengke Pan and  
492 Pan Liu performed the analysis and wrote the paper. Shida Gao, Jun Xia, Jie Chen and  
493 Lei Cheng contributed to the writing of the paper and made comments.

#### 494 **COMPLIANCE WITH ETHICAL STANDARDS**

495 **Conflict of interest:** The authors declare that they have no conflict of interest.

#### 496 **REFERENCES**

- 497 Ajami, N. K., Duan, Q. Y., and Sorooshian, S.: An integrated hydrologic Bayesian multimodel  
498 combination framework: Confronting input, parameter, and model structural uncertainty  
499 in hydrologic prediction, *Water Resour. Res.*, 43, 10.1029/2005wr004745, 2007.
- 500 Bracken, C., Holman, K. D., Rajagopalan, B., and Moradkhani, H.: A Bayesian Hierarchical  
501 Approach to Multivariate Nonstationary Hydrologic Frequency Analysis, *Water Resour.*  
502 *Res.*, 54, 243-255, 10.1002/2017wr020403, 2018.
- 503 Brigode, P., Oudin, L., and Perrin, C.: Hydrological model parameter instability: A source of  
504 additional uncertainty in estimating the hydrological impacts of climate change?, *J.*  
505 *Hydrol.*, 476, 410-425, 10.1016/j.jhydrol.2012.11.012, 2013.
- 506 Broderick, C., Matthews, T., Wilby, R. L., Bastola, S., and Murphy, C.: Transferability of  
507 hydrological models and ensemble averaging methods between contrasting climatic  
508 periods, *Water Resour. Res.*, 52, 8343-8373, 10.1002/2016wr018850, 2016.
- 509 Cha, Y., Park, S. S., Lee, H. W., and Stow, C. A.: A Bayesian hierarchical approach to model  
510 seasonal algal variability along an upstream to downstream river gradient, *Water Resour.*  
511 *Res.*, 52, 348-357, 10.1002/2015wr017327, 2016.
- 512 Chen, X., Hao, Z., Devineni, N., and Lall, U.: Climate information based streamflow and rainfall



- 513 forecasts for Huai River basin using hierarchical Bayesian modeling, *Hydrol. Earth Syst.*  
514 *Sci.*, 18, 1539-1548, 10.5194/hess-18-1539-2014, 2014.
- 515 Chiew, F. H. S., Teng, J., Vaze, J., Post, D. A., Perraud, J. M., Kirono, D. G. C., and Viney, N. R.:  
516 Estimating climate change impact on runoff across southeast Australia: Method, results,  
517 and implications of the modeling method, *Water Resour. Res.*, 45, 17,  
518 10.1029/2008wr007338, 2009.
- 519 Chiew, F. H. S., Potter, N. J., Vaze, J., Petheram, C., Zhang, L., Teng, J., and Post, D. A.: Observed  
520 hydrologic non-stationarity in far south-eastern Australia: implications for modelling and  
521 prediction, *Stoch. Environ. Res. Risk Assess.*, 28, 3-15, 10.1007/s00477-013-0755-5, 2014.
- 522 Ciais, P., Reichstein, M., Viovy, N., Granier, A., Ogee, J., Allard, V., Aubinet, M., Buchmann, N.,  
523 Bernhofer, C., Carrara, A., Chevallier, F., De Noblet, N., Friend, A. D., Friedlingstein, P.,  
524 Grunwald, T., Heinesch, B., Keronen, P., Knohl, A., Krinner, G., Loustau, D., Manca, G.,  
525 Matteucci, G., Miglietta, F., Ourcival, J. M., Papale, D., Pilegaard, K., Rambal, S., Seufert,  
526 G., Soussana, J. F., Sanz, M. J., Schulze, E. D., Vesala, T., and Valentini, R.: Europe-wide  
527 reduction in primary productivity caused by the heat and drought in 2003, *Nature*, 437,  
528 529-533, 10.1038/nature03972, 2005.
- 529 Clarke, R. T.: Hydrological prediction in a non-stationary world, *Hydrol. Earth Syst. Sci.*, 11, 408-  
530 414, 10.5194/hess-11-408-2007, 2007.
- 531 Cook, E. R., Woodhouse, C. A., Eakin, C. M., Meko, D. M., and Stahle, D. W.: Long-term aridity  
532 changes in the western United States, *Science*, 306, 1015-1018,  
533 10.1126/science.1102586, 2004.
- 534 Cooley, D., Nychka, D., and Naveau, P.: Bayesian spatial modeling of extreme precipitation  
535 return levels, *J. Am. Stat. Assoc.*, 102, 824-840, 10.1198/016214506000000780, 2007.
- 536 Coron, L., Andreassian, V., Perrin, C., Lerat, J., Vaze, J., Bourqui, M., and Hendrickx, F.: Crash  
537 testing hydrological models in contrasted climate conditions: An experiment on 216  
538 Australian catchments, *Water Resour. Res.*, 48, 17, 10.1029/2011wr011721, 2012.
- 539 Deng, C., Liu, P., Guo, S. L., Li, Z. J., and Wang, D. B.: Identification of hydrological model  
540 parameter variation using ensemble Kalman filter, *Hydrol. Earth Syst. Sci.*, 20, 4949-4961,  
541 10.5194/hess-20-4949-2016, 2016.
- 542 Deng, C., Liu, P., Wang, D. B., and Wang, W. G.: Temporal variation and scaling of parameters  
543 for a monthly hydrologic model, *J. Hydrol.*, 558, 290-300, 10.1016/j.jhydrol.2018.01.049,  
544 2018.
- 545 Duan, Q. Y., Ajami, N. K., Gao, X. G., and Sorooshian, S.: Multi-model ensemble hydrologic  
546 prediction using Bayesian model averaging, *Adv. Water Resour.*, 30, 1371-1386,  
547 10.1016/j.advwatres.2006.11.014, 2007.
- 548 Fowler, K. J. A., Peel, M. C., Western, A. W., Zhang, L., and Peterson, T. J.: Simulating runoff  
549 under changing climatic conditions: Revisiting an apparent deficiency of conceptual  
550 rainfall-runoff models, *Water Resour. Res.*, 52, 1820-1846, 10.1002/2015wr018068, 2016.
- 551 Gelman, A., Carlin, J., Stern, H., Dunson, D., Vehtari, A., and Rubin, D.: *Bayesian Data Analysis*,  
552 third ed ed., CRC Press, 2013.
- 553 Guo, D. L., Westra, S., and Maier, H. R.: Impact of evapotranspiration process representation  
554 on runoff projections from conceptual rainfall-runoff models, *Water Resour. Res.*, 53, 435-  
555 454, 10.1002/2016wr019627, 2017.
- 556 Heuvelmans, G., Muys, B., and Feyen, J.: Regionalisation of the parameters of a hydrological





- 557 model: Comparison of linear regression models with artificial neural nets, *J. Hydrol.*, 319,  
558 245-265, [10.1016/j.jhydrol.2005.07.030](https://doi.org/10.1016/j.jhydrol.2005.07.030), 2006.
- 559 Lebecherel, L., Andreassian, V., and Perrin, C.: On evaluating the robustness of spatial-  
560 proximity-based regionalization methods, *J. Hydrol.*, 539, 196-203,  
561 [10.1016/j.jhydrol.2016.05.031](https://doi.org/10.1016/j.jhydrol.2016.05.031), 2016.
- 562 Lima, C. H. R., and Lall, U.: Hierarchical Bayesian modeling of multisite daily rainfall occurrence:  
563 Rainy season onset, peak, and end, *Water Resour. Res.*, 45, 14, [10.1029/2008wr007485](https://doi.org/10.1029/2008wr007485),  
564 2009.
- 565 Lima, C. H. R., Lall, U., Troy, T., and Devineni, N.: A hierarchical Bayesian GEV model for  
566 improving local and regional flood quantile estimates, *J. Hydrol.*, 541, 816-823,  
567 [10.1016/j.jhydrol.2016.07.042](https://doi.org/10.1016/j.jhydrol.2016.07.042), 2016.
- 568 Liu, P., Li, L. P., Chen, G. J., and Rheinheimer, D. E.: Parameter uncertainty analysis of reservoir  
569 operating rules based on implicit stochastic optimization, *J. Hydrol.*, 514, 102-113,  
570 [10.1016/j.jhydrol.2014.04.012](https://doi.org/10.1016/j.jhydrol.2014.04.012), 2014.
- 571 Liu, Y. Q., and Gupta, H. V.: Uncertainty in hydrologic modeling: Toward an integrated data  
572 assimilation framework, *Water Resour. Res.*, 43, 18, [10.1029/2006wr005756](https://doi.org/10.1029/2006wr005756), 2007.
- 573 Merz, R., and Blöschl, G.: Regionalisation of catchment model parameters, *J. Hydrol.*, 287, 95-  
574 123, [10.1016/j.jhydrol.2003.09.028](https://doi.org/10.1016/j.jhydrol.2003.09.028), 2004.
- 575 Merz, R., Parajka, J., and Blöschl, G.: Time stability of catchment model parameters:  
576 Implications for climate impact analyses, *Water Resour. Res.*, 47, 17,  
577 [10.1029/2010wr009505](https://doi.org/10.1029/2010wr009505), 2011.
- 578 Moore, R. D., and Wondzell, S. M.: Physical hydrology and the effects of forest harvesting in  
579 the Pacific Northwest: A review, *J. Am. Water Resour. Assoc.*, 41, 763-784, 2005.
- 580 Moradkhani, H., Hsu, K. L., Gupta, H., and Sorooshian, S.: Uncertainty assessment of hydrologic  
581 model states and parameters: Sequential data assimilation using the particle filter, *Water  
582 Resour. Res.*, 41, 17, [10.1029/2004wr003604](https://doi.org/10.1029/2004wr003604), 2005.
- 583 Moradkhani, H., DeChant, C. M., and Sorooshian, S.: Evolution of ensemble data assimilation  
584 for uncertainty quantification using the particle filter-Markov chain Monte Carlo method,  
585 *Water Resour. Res.*, 48, 13, [10.1029/2012wr012144](https://doi.org/10.1029/2012wr012144), 2012.
- 586 Moriasi, D. N., Arnold, J. G., Van Liew, M. W., Bingner, R. L., Harmel, R. D., and Veith, T. L.: Model  
587 evaluation guidelines for systematic quantification of accuracy in watershed simulations,  
588 *Trans. ASABE*, 50, 885-900, 2007.
- 589 Najafi, M. R., and Moradkhani, H.: A hierarchical Bayesian approach for the analysis of climate  
590 change impact on runoff extremes, *Hydrol. Process.*, 28, 6292-6308, [10.1002/hyp.10113](https://doi.org/10.1002/hyp.10113),  
591 2014.
- 592 Nash, J. E., and Sutcliffe, J. V.: River flow forecasting through conceptual models part I — A  
593 discussion of principles, *J. Hydrol.*, 10, 282-290, [https://doi.org/10.1016/0022-  
594 1694\(70\)90255-6](https://doi.org/10.1016/0022-1694(70)90255-6), 1970.
- 595 Oudin, L., Andreassian, V., Perrin, C., Michel, C., and Le Moine, N.: Spatial proximity, physical  
596 similarity, regression and ungaged catchments: A comparison of regionalization  
597 approaches based on 913 French catchments, *Water Resour. Res.*, 44, 15,  
598 [10.1029/2007wr006240](https://doi.org/10.1029/2007wr006240), 2008.
- 599 Pathiraja, S., Marshall, L., Sharma, A., and Moradkhani, H.: Detecting non-stationary hydrologic  
600 model parameters in a paired catchment system using data assimilation, *Adv. Water*



- 601 Resour., 94, 103-119, 10.1016/j.advwatres.2016.04.021, 2016.
- 602 Pathiraja, S., Moradkhani, H., Marshall, L., Sharma, A., and Geenens, G.: Data-Driven Model  
603 Uncertainty Estimation in Hydrologic Data Assimilation, *Water Resour. Res.*, 54, 1252-  
604 1280, 10.1002/2018wr022627, 2018.
- 605 Patil, S. D., and Stieglitz, M.: Comparing Spatial and temporal transferability of hydrological  
606 model parameters, *J. Hydrol.*, 525, 409-417, 10.1016/j.jhydrol.2015.04.003, 2015.
- 607 Perrin, C., Michel, C., and Andreassian, V.: Improvement of a parsimonious model for  
608 streamflow simulation, *J. Hydrol.*, 279, 275-289, 10.1016/s0022-1694(03)00225-7, 2003.
- 609 Renard, B., Kavetski, D., Leblois, E., Thyer, M., Kuczera, G., and Franks, S. W.: Toward a reliable  
610 decomposition of predictive uncertainty in hydrological modeling: Characterizing rainfall  
611 errors using conditional simulation, *Water Resour. Res.*, 47, 21, 10.1029/2011wr010643,  
612 2011.
- 613 Saft, M., Western, A. W., Zhang, L., Peel, M. C., and Potter, N. J.: The influence of multiyear  
614 drought on the annual rainfall-runoff relationship: An Australian perspective, *Water  
615 Resour. Res.*, 51, 2444-2463, 10.1002/2014wr015348, 2015.
- 616 Seiller, G., Anctil, F., and Perrin, C.: Multimodel evaluation of twenty lumped hydrological  
617 models under contrasted climate conditions, *Hydrol. Earth Syst. Sci.*, 16, 1171-1189,  
618 10.5194/hess-16-1171-2012, 2012.
- 619 Singh, S. K., Bardossy, A., Gotzinger, J., and Sudheer, K. P.: Effect of spatial resolution on  
620 regionalization of hydrological model parameters, *Hydrol. Process.*, 26, 3499-3509,  
621 10.1002/hyp.8424, 2012.
- 622 Spiegelhalter, D. J., Best, N. G., Carlin, B. R., and van der Linde, A.: Bayesian measures of model  
623 complexity and fit, *J. R. Stat. Soc. Ser. B-Stat. Methodol.*, 64, 583-616, 10.1111/1467-  
624 9868.00353, 2002.
- 625 Sun, X., Thyer, M., Renard, B., and Lang, M.: A general regional frequency analysis framework  
626 for quantifying local-scale climate effects: A case study of ENSO effects on Southeast  
627 Queensland rainfall, *J. Hydrol.*, 512, 53-68, 10.1016/j.jhydrol.2014.02.025, 2014.
- 628 Sun, X., and Lall, U.: Spatially coherent trends of annual maximum daily precipitation in the  
629 United States, *Geophys. Res. Lett.*, 42, 9781-9789, 10.1002/2015gl066483, 2015.
- 630 Sun, X., Lall, U., Merz, B., and Dung, N. V.: Hierarchical Bayesian clustering for nonstationary  
631 flood frequency analysis: Application to trends of annual maximum flow in Germany,  
632 *Water Resour. Res.*, 51, 6586-6601, 10.1002/2015wr017117, 2015.
- 633 Tegegne, G., and Kim, Y. O.: Modelling ungauged catchments using the catchment runoff  
634 response similarity, *J. Hydrol.*, 564, 452-466, 10.1016/j.jhydrol.2018.07.042, 2018.
- 635 Thirel, G., Andreassian, V., Perrin, C., Audouy, J. N., Berthet, L., Edwards, P., Folton, N., Furusho,  
636 C., Kuentz, A., Lerat, J., Lindstrom, G., Martin, E., Mathevet, T., Merz, R., Parajka, J.,  
637 Ruelland, D., and Vaze, J.: Hydrology under change: an evaluation protocol to investigate  
638 how hydrological models deal with changing catchments, *Hydrol. Sci. J.-J. Sci. Hydrol.*, 60,  
639 1184-1199, 10.1080/02626667.2014.967248, 2015.
- 640 Vaze, J., Post, D. A., Chiew, F. H. S., Perraud, J. M., Viney, N. R., and Teng, J.: Climate non-  
641 stationarity - Validity of calibrated rainfall-runoff models for use in climate change studies,  
642 *J. Hydrol.*, 394, 447-457, 10.1016/j.jhydrol.2010.09.018, 2010.
- 643 Vrugt, J. A., Gupta, H. V., Bouten, W., and Sorooshian, S.: A Shuffled Complex Evolution  
644 Metropolis algorithm for optimization and uncertainty assessment of hydrologic model



- 645 parameters, *Water Resour. Res.*, 39, 18, 10.1029/2002wr001642, 2003.
- 646 Vrugt, J. A., ter Braak, C. J. F., Diks, C. G. H., Robinson, B. A., Hyman, J. M., and Higdon, D.:  
647 Accelerating Markov Chain Monte Carlo Simulation by Differential Evolution with Self-  
648 Adaptive Randomized Subspace Sampling, *International Journal of Nonlinear Sciences*  
649 *and Numerical Simulation*, 10, 273-290, 2009.
- 650 Westra, S., Thyer, M., Leonard, M., Kavetski, D., and Lambert, M.: A strategy for diagnosing and  
651 interpreting hydrological model nonstationarity, *Water Resour. Res.*, 50, 5090-5113,  
652 10.1002/2013wr014719, 2014.
- 653 Wright, D. P., Thyer, M., and Westra, S.: Influential point detection diagnostics in the context  
654 of hydrological model calibration, *J. Hydrol.*, 527, 1161-1172,  
655 10.1016/j.jhydrol.2015.05.047, 2015.
- 656 Xiong, M., Liu, P., Cheng, L., Deng, C., Gui, Z., Zhang, X., and Liu, Y.: Identifying time-varying  
657 hydrological model parameters to improve simulation efficiency by the ensemble Kalman  
658 filter: A joint assimilation of streamflow and actual evapotranspiration, *J. Hydrol.*, 568,  
659 758-768, 10.1016/j.jhydrol.2018.11.038, 2019.
- 660 Xu, Q., Chen, J., Peart, M. R., Ng, C. N., Hau, B. C. H., and Law, W. W. Y.: Exploration of severities  
661 of rainfall and runoff extremes in ungauged catchments: A case study of Lai Chi Wo in  
662 Hong Kong, China, *Sci. Total Environ.*, 634, 640-649, 10.1016/j.scitotenv.2018.04.024,  
663 2018.
- 664 Yan, H. X., and Moradkhani, H.: A regional Bayesian hierarchical model for flood frequency  
665 analysis, *Stoch. Environ. Res. Risk Assess.*, 29, 1019-1036, 10.1007/s00477-014-0975-3,  
666 2015.
- 667 Zhang, X. J., Liu, P., Cheng, L., Liu, Z. J., and Zhao, Y.: A back-fitting algorithm to improve real-  
668 time flood forecasting, *J. Hydrol.*, 562, 140-150, 10.1016/j.jhydrol.2018.04.051, 2018.
- 669 Zhang, Y. Q., Viney, N., Frost, A., and Oke, A.: Collation of Australian modeller's streamflow  
670 dataset for 780 unregulated Australian catchments, *Water for a healthy country national*  
671 *research flagship*, 115pp, 2013.
- 672



673 **TABLES**

674 **Table 1. Different spatial coherence scenarios for regression parameters  $\beta$  and  $\omega$  in the time-varying functional form of model parameter**  
 675  **$\theta_1$ . To explore the performance of spatial coherence within the time-varying function, different levels of spatial coherence for regression**  
 676 **parameters  $\beta$  and  $\omega$  were assumed for the first three scenarios; in contrast, no spatial coherence is assumed in scenario 4, and a temporally**  
 677 **stable  $\theta_1$  is assumed in scenario 5.**

Category	Scenario	$\beta$	$\omega$	Constraints
Time-varying	1	Parameter $\beta$ is region-related	Parameter $\omega$ is catchment-specific	$\theta_1 = \alpha(c) + \beta(c) + \sin[\omega(c)]$ , while $\beta(c) = N(\mu_2, \sigma_2^2)$
	2	Parameter $\beta$ is catchment-specific	Parameter $\omega$ is region-related	$\theta_1 = \alpha(c) + \beta(c) + \sin[\omega(c)]$ , while $\omega(c) = N(\mu_3, \sigma_3^2)$
	3	Parameter $\beta$ is region-related	Parameter $\omega$ is region-related	$\theta_1 = \alpha(c) + \beta(c) + \sin[\omega(c)]$ , while $\beta(c) = N(\mu_2, \sigma_2^2)$ and $\omega(c) = N(\mu_3, \sigma_3^2)$
	4	Parameter $\beta$ is catchment-specific	Parameter $\omega$ is catchment-specific	$\theta_1 = \alpha(c) + \beta(c) + \sin[\omega(c)]$
	5	No parameters $\beta$ or $\omega$	No parameters $\beta$ or $\omega$	$\theta_1$ is stationary

678

679 NB:  $\theta_1$  is the production storage capacity of the catchment;  $\beta$  is the slope describing long-term change during the modeling period, and  $\omega$  is the amplitude of the sine  
 680 function describing its seasonal variation during the modeling period;  $\mu_2, \sigma_2, \mu_3, \sigma_3$  are hyper-parameters.



681 **Table 2. Comparison of catchments attributes in terms of mean annual rainfall (mm), mean annual evaporation (mm), and mean annual**  
 682 **runoff (mm) for 1976–2011.**  
 683

Catchments ID	River Name	Observations start	Observations end	Mean annual rainfall	Mean annual potential evapotranspiration	Mean annual runoff
225219	Macalister	1/1/1976	30/12/2011	1064	1142	350
405219	Goulburn	1/1/1976	30/12/2011	1169	1193	422
405264	Big	1/1/1976	30/12/2011	1406	1157	469

684 **Table 3. Drought identification results for the catchments.**  
 685

Catchments ID	Drought start	Drought end	Length	Mean dry period anomaly	% Complete	R <sub>1</sub>	R <sub>2</sub>	Change in runoff (%)	Change in rainfall (%)
225219	1997	2009	12	-6.95%	90.4%	0.34	0.28	-15.98	-11.27
405219	1997	2009	12	-9.84%	98.5%	0.38	0.31	-18.57	-10.97
405264	1997	2009	12	-9.62%	98.5%	0.35	0.29	-18.23	-10.51

686 NB: R<sub>1</sub> and R<sub>2</sub> refer to the runoff coefficient during the non-dry and dry periods, respectively.

687  
 688  
 689  
 690  
 691  
 692  
 693



694 **Table 4. Comparison of five scenarios in terms of the deviance information**  
 695 **criterion (DIC) when model parameters were calibrated in the non-dry period and**  
 696 **verified in the dry period.**  
 697

Category		Scenario	DIC
Time-varying	Spatial coherence	1	4961.7
		2	1202.3
		3	-1254.4
Time invariant	No spatial coherence	4	5052.8
		5	5827.3

698

699 **Table 5. Comparison of five scenarios in terms of the deviance information**  
 700 **criterion (DIC) when model parameters were calibrated in the dry period and**  
 701 **verified in the non-dry period.**  
 702

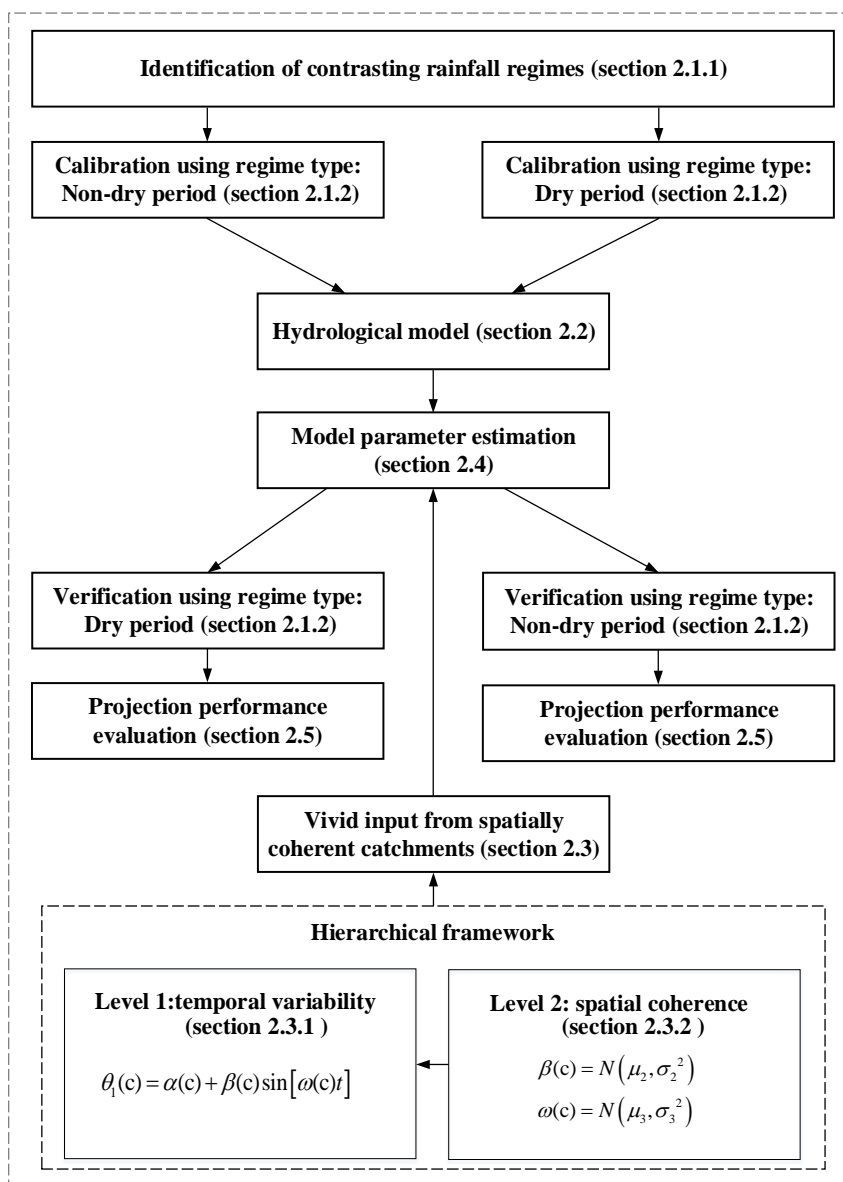
Category		Scenario	DIC
Time-varying	Spatial coherence	1	-6167.0
		2	-5743.6
		3	-10574.0
Time invariant	No spatial coherence	4	-8710.0
		5	-7460.8

703

704



705 **FIGURES**



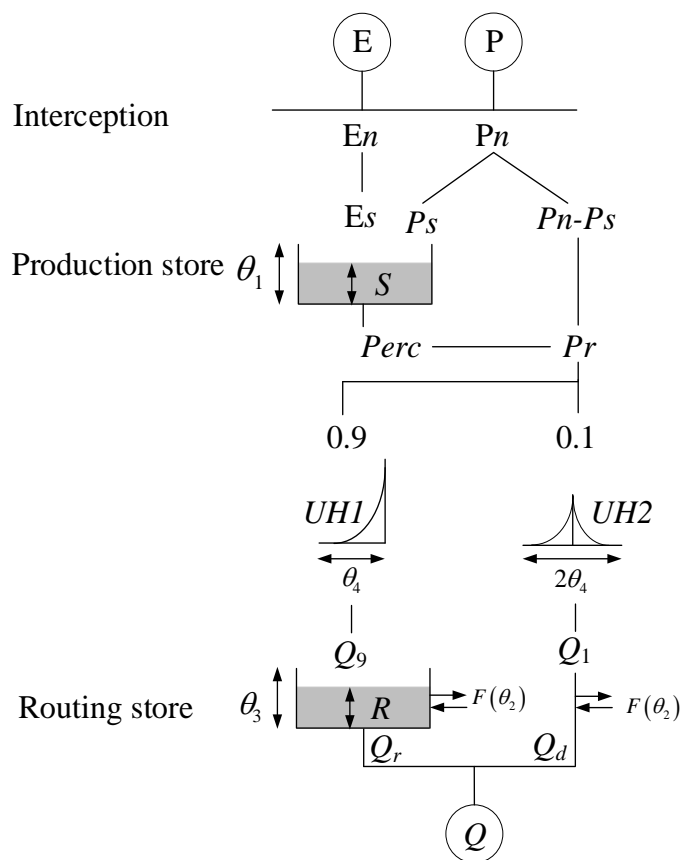
706

707 **Figure 1. Flow diagram of the methodology for integrating inputs from spatially**  
 708 **coherent catchments and temporal variation of model parameters into a**  
 709 **hydrological model under contrasting climatic conditions (non-dry and dry**  
 710 **periods).**

711



712

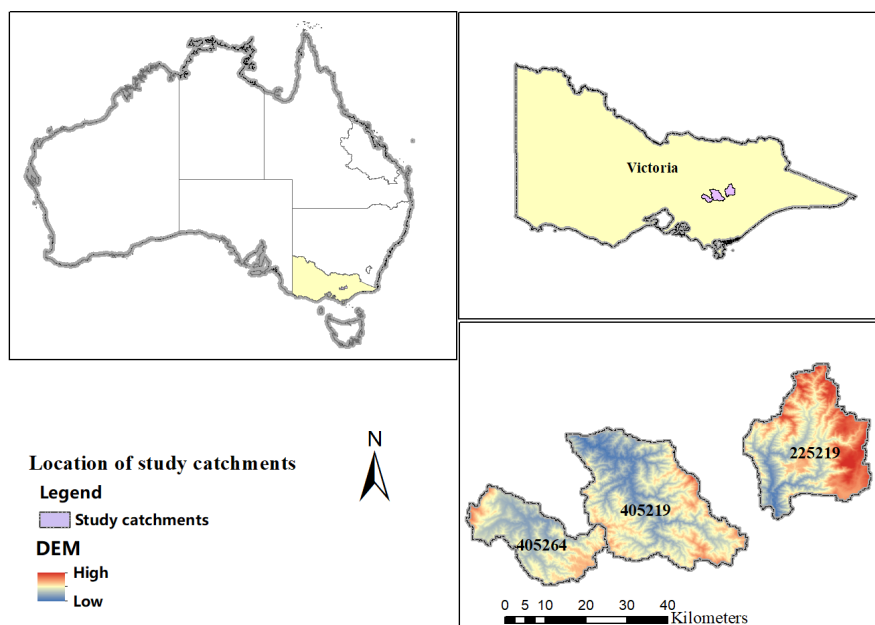


713

714 **Figure 2. Schematic of the original version of the GR4J rainfall-runoff model.**

715





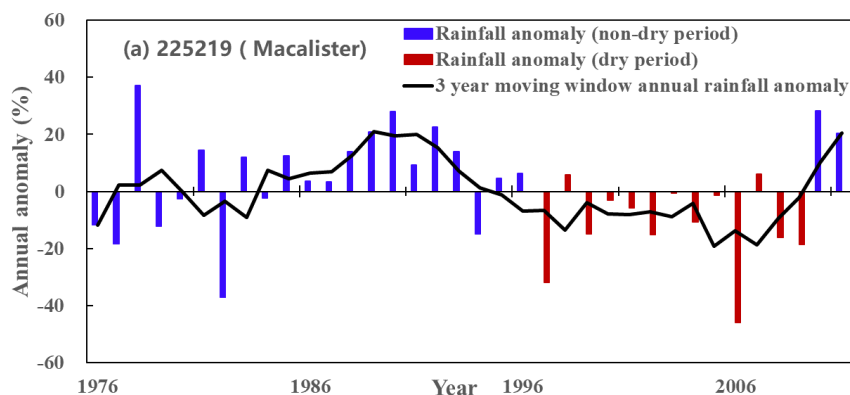
716

717 **Figure 3. Locations of study catchments in Victoria, Australia. The catchment IDs**  
718 **are 225219 (Macalister River catchment), 405219 (Goulburn River catchment),**  
719 **and 405264 (Big River catchment).**

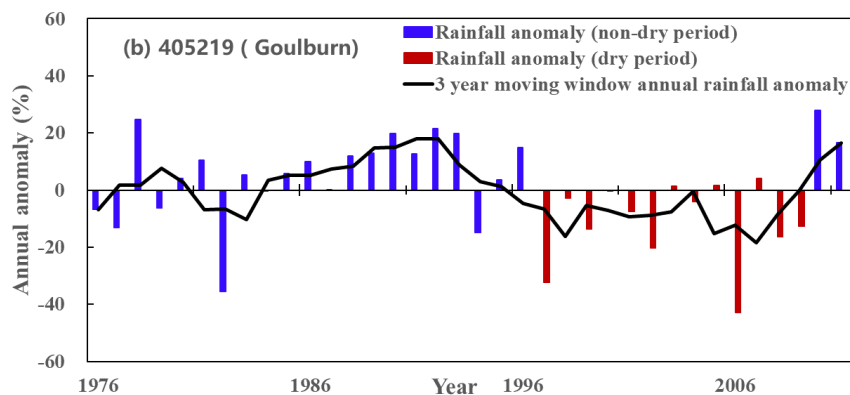
720

721

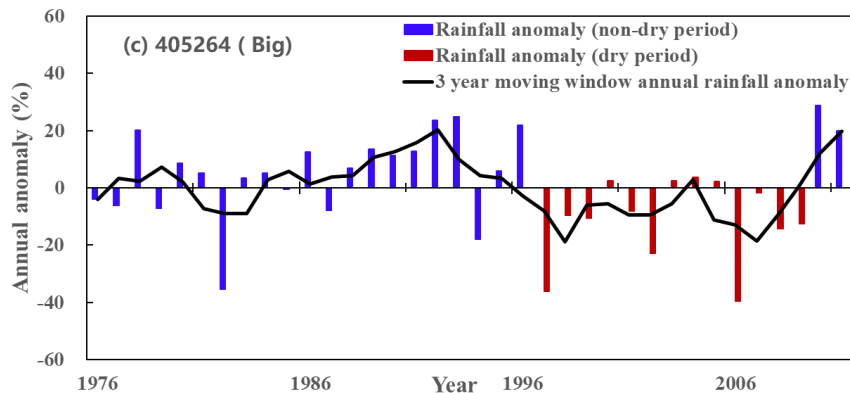
722



723



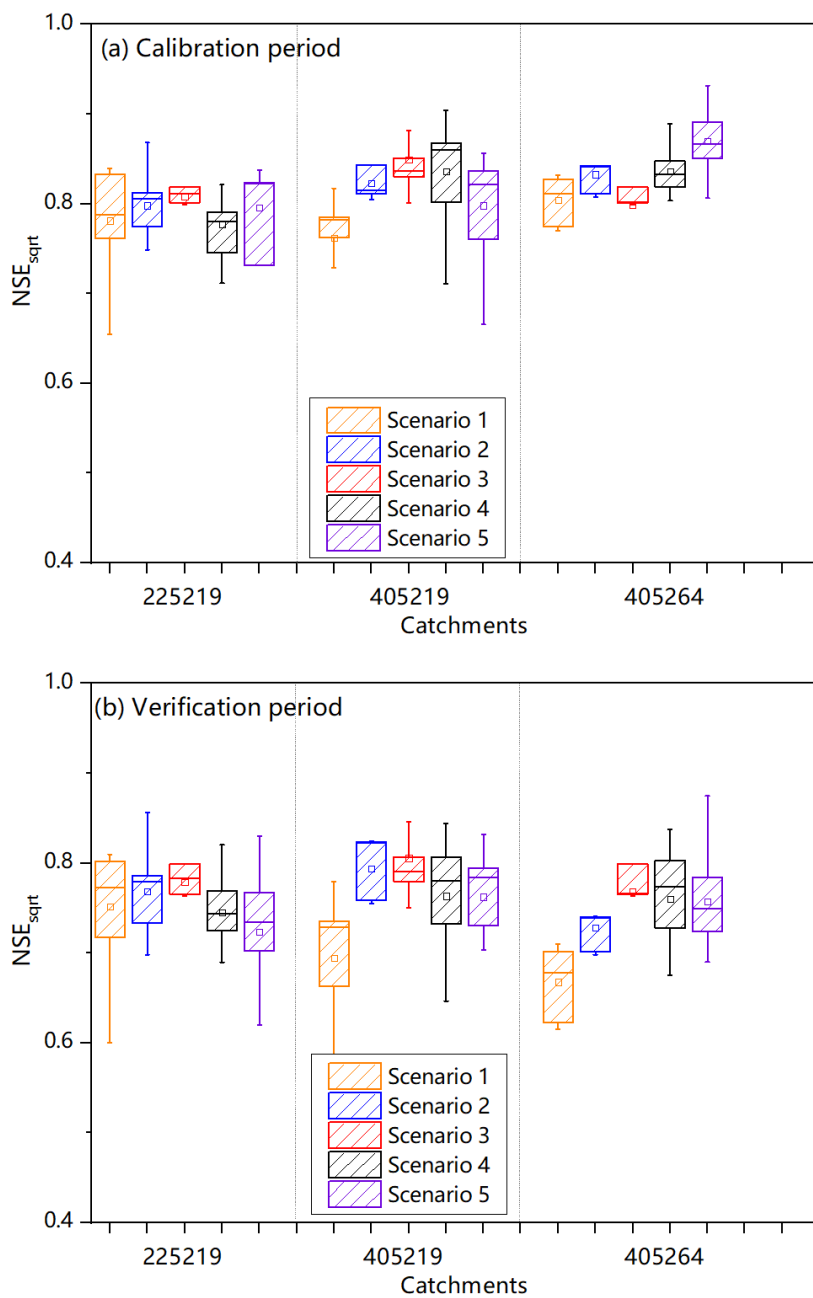
724



725

726 **Figure 4. The identified dry period in all catchments. The annual anomaly is**  
727 **defined as a percentage of the mean annual rainfall.**

728



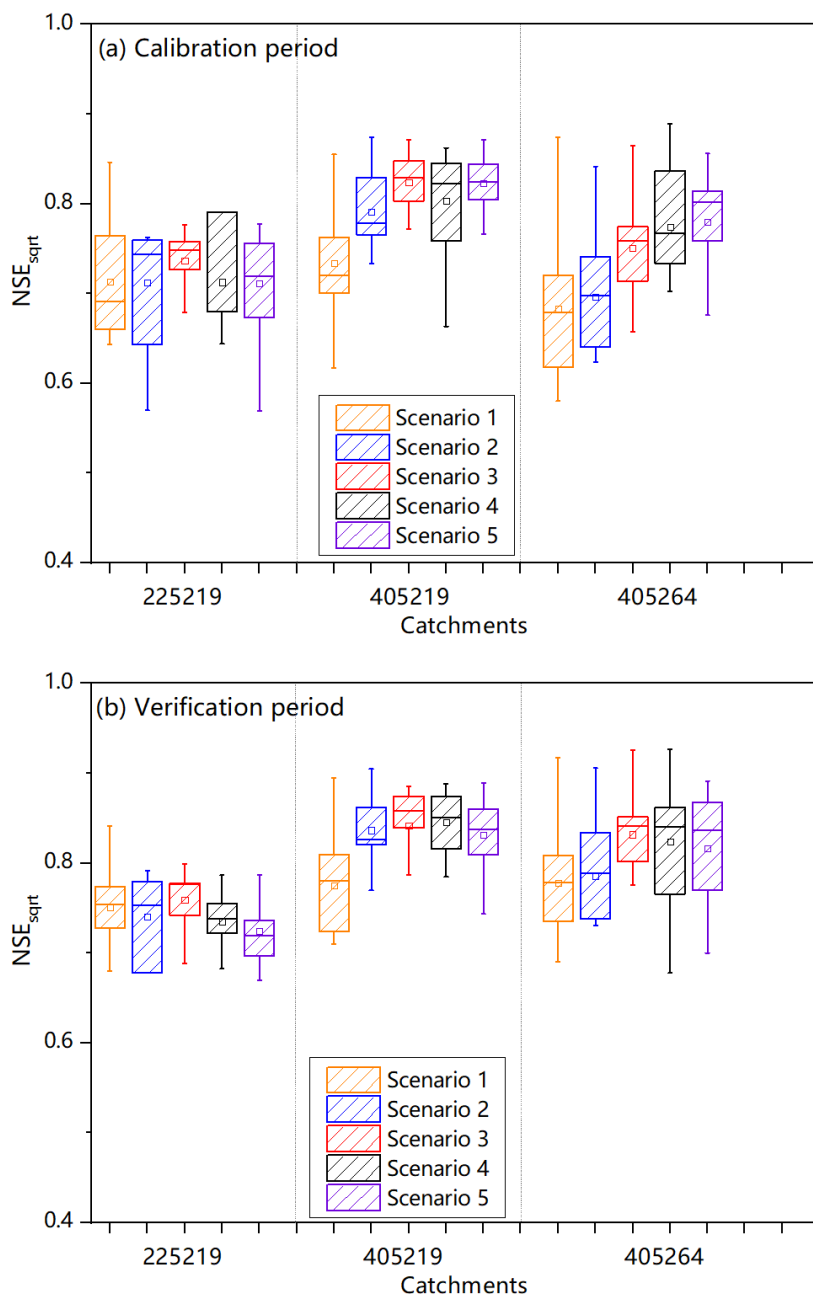
729

730

731

732

**Figure 5.  $NSE_{sqrt}$  for each of the five scenarios for each catchment during (a) the calibration period (non-dry period) and (b) the verification period (dry period).**



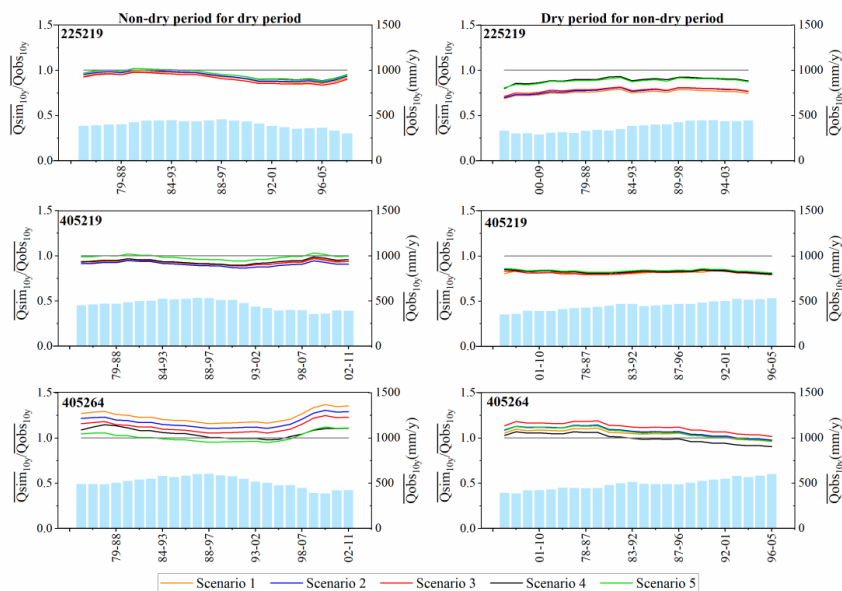
733

734

735

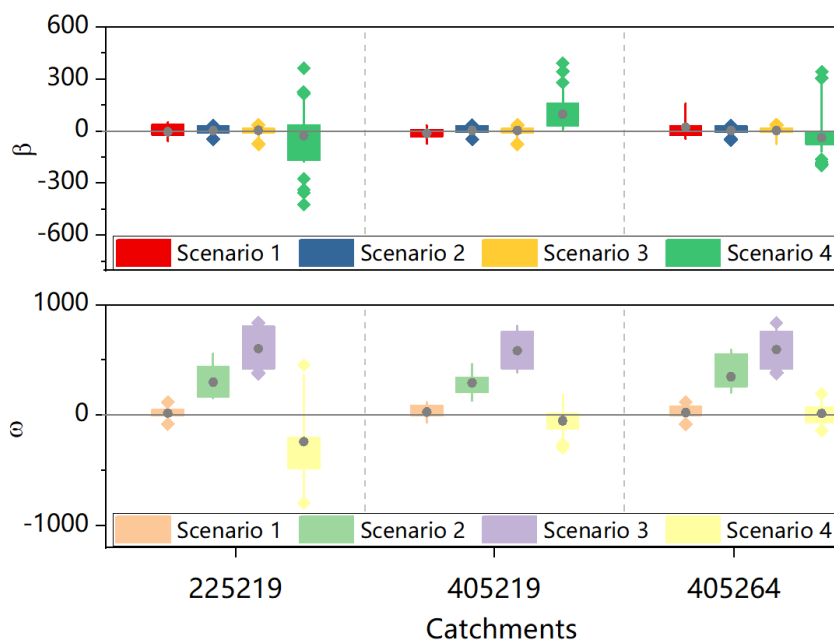
736

**Figure 6. NSE<sub>sqrt</sub> for each of the five scenarios for each catchment during (a) the calibration period (dry period) and (b) the verification period (non-dry period).**



737

738 **Figure 7. Long-term simulation BIAS of  $Q_{\text{median}}$  for five scenarios in all catchments.**  
 739 **Simulation BIAS is plotted as a 10-year moving average, and 10-year moving**  
 740 **average streamflows are plotted for reference. The left-hand three graphs are**  
 741 **calibrated in the non-dry period and then verified in the dry period, while the**  
 742 **opposite sequence applies to the right-hand graphs.**  
 743

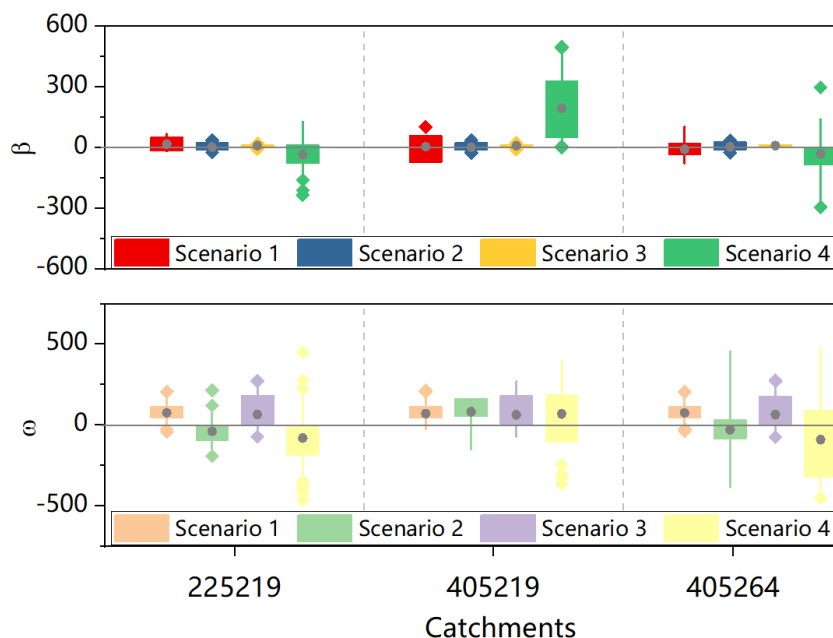


744

745 **Figure 8. Posterior distributions of the regression parameters ( $\beta$  and  $\omega$ ) for the**  
 746 **production storage capacity ( $\theta_1$ ) for the four model scenarios in each catchment**  
 747 **when calibrated in the non-dry period and verified in the dry period. Upper and**  
 748 **lower ranges are given by the 25<sup>th</sup> and 75<sup>th</sup> percentiles of the posterior distribution.**  
 749 **The whiskers extend to values defining 1.5-standard deviations of the sample.**  
 750 **Small dots (gray) denote the arithmetic average of the posterior distribution of**  
 751 **this parameter. Values beyond the whiskers are marked as outliers and denoted as**  
 752 **small squares.**

753

754



755  
 756 **Figure 9. Posterior distributions of the regression parameters ( $\beta$  and  $\omega$ ) for the**  
 757 **production storage capacity ( $\theta_1$ ) for the first four model scenarios in each**  
 758 **catchment when calibrated in the dry period and verified in the non-dry period.**  
 759 **Upper and lower ranges are given by the 25<sup>th</sup> and 75<sup>th</sup> percentiles of the posterior**  
 760 **distribution. The whiskers extend to values defining 1.5-standard deviations of the**  
 761 **sample. Small dots (gray) denote the arithmetic average of the posterior**  
 762 **distribution of this parameter. Values beyond the whiskers are marked as outliers**  
 763 **and denoted as small squares.**  
 764